



# Thermo-kinetic modelling of the giant Snoek effect in carbon-supersaturated iron

Philippe Maugis

## ► To cite this version:

Philippe Maugis. Thermo-kinetic modelling of the giant Snoek effect in carbon-supersaturated iron. Journal of Alloys and Compounds, 2021, 877, pp.160236. 10.1016/j.jallcom.2021.160236 . hal-03600560

**HAL Id: hal-03600560**

**<https://hal.science/hal-03600560>**

Submitted on 7 Mar 2022

**HAL** is a multi-disciplinary open access archive for the deposit and dissemination of scientific research documents, whether they are published or not. The documents may come from teaching and research institutions in France or abroad, or from public or private research centers.

L'archive ouverte pluridisciplinaire **HAL**, est destinée au dépôt et à la diffusion de documents scientifiques de niveau recherche, publiés ou non, émanant des établissements d'enseignement et de recherche français ou étrangers, des laboratoires publics ou privés.

# Thermo-kinetic modelling of the giant Snoek effect in carbon-supersaturated iron

Philippe Maugis<sup>a,\*</sup>

<sup>a</sup>Aix Marseille Univ, CNRS, IM2NP, Marseille, France

## ARTICLE INFO

### Keywords:

anelastic behaviour  
internal friction  
long-range ordering  
carbon steels

## ABSTRACT

Snoek relaxation in interstitial bcc solid solutions is the origin of the Snoek peak in frequency-dependent and temperature-dependent internal friction measurements. When applied to low-carbon steels, the internal friction profiles show a linear dependence of the peak height with carbon content. However, recent Monte Carlo simulations of frequency-dependent internal friction exhibited a non-linear giant peak height at high carbon contents. To investigate this effect in temperature-dependent internal friction, we developed a thermo-kinetic mean-field theory of the Snoek relaxation phenomenon. By taking into account the collective behaviour of the interstitial atoms, our theory predicts (i) a non-linear dependence of the peak height with composition when approaching the order–disorder transition of the alloy; (ii) a shift in the temperature of the peak; (iii) a composition-dependent activation enthalpy of the relaxation time. The theory is exemplified by the case of carbon-supersaturated iron.

## 1. Introduction

The Snoek effect in body-centred solid solutions originates from the tendency of interstitial atoms to occupy specific non-equivalent sites in strained crystals: the elastic strain field energetically favours one of the three sets of interstitial sites, inducing a redistribution of the interstitial atoms via atomic jumps towards the favoured sites. Now, as each interstitial deforms the host matrix, the homogeneous strain of the crystal results not only from the applied stress but also from the distribution of the interstitial atoms over the atomic sites. This strain in turn interacts with the interstitial atoms and affects the energetic levels of both stable and transition sites. The thermodynamics of the solid solution as well as the kinetics of the atomic jumps are thus affected by both the applied stress and the interstitial distribution.

In 1948, Zener [1] showed that the alloy thermodynamics based on carbon–strain interaction in a stress-free Fe-C crystal leads to carbon long-range ordering below a transition temperature. By a mean-field model, Shtremel [2] showed that an applied stress can favour Zener ordering. These ideas have been confirmed since by various theoretical approaches [3–19]. The effect can be understood as follows: an applied stress creates a strain (the elastic response) that favours one set of octahedral sites. These sites becoming progressively over-populated create an additional strain (the anelastic response) that in turn favours the sites even more. As a result, when applied to a low-carbon alloy, the stress induces a low-order state, the ferrite phase; above a threshold carbon content, it produces a high-order state, the martensite phase. In the vicinity of the threshold composition, the collective response of the carbon atoms produces a very large anelastic strain response, which is the origin of the giant Snoek effect [20, 21].


The carbon–carbon long-range elastic interaction therefore modifies the Snoek relaxation behaviour. Several theoretical works have focused on this point. The coupling model [22–24] is derived from a mean-field approximation of the elasticity theory of point defects. The random cooperative strain interaction model (RCSI) [25] assumes a random distribution of the strain interactions. These models predict a shift and a broadening of the internal friction profiles. However, they do not consider the consequence of long-range carbon–carbon interaction on the saddle point energy of the jumping atoms. Recently, the author showed by Monte Carlo simulations that this interaction has a strong effect on the relaxation time [21].


In this paper, we present a mean-field approach of the Snoek relaxation phenomenon. Our theory is based on the elastochemical model describing the thermodynamics of the interstitial solid solution [26], and on the rate theory applied to carbon jumps [18, 27, 28]. Both thermodynamic and kinetic aspects rely on the elasticity theory of point defects to describe the long-range carbon–carbon interaction. This thermo-kinetic model is applied to internal friction measurements. Our results are compared to Monte Carlo simulations of frequency-dependent profiles and to an experimental temperature-dependent profile. The focus is then set on the effect of carbon content on the internal friction. The non-linear peak height–carbon content relationship and the giant Snoek effect in supersaturated alloys are highlighted. The limits of the standard linear-response approximation [29] are also discussed.

## 2. The thermo-kinetic model

The thermo-kinetic model is a consistent description of the thermodynamics of carbon long-range ordering and of the dynamics of carbon atomic jumps. As was demonstrated in previous papers [6, 19], Zener ordering mostly depends on the long-range elastic carbon–carbon interactions. Therefore, short-range interactions can be neglected. The mean-

\*Corresponding author

 philippe.maugis@univ-amu.fr (P. Maugis)

 www.im2np.fr (P. Maugis)

ORCID(s): 0000-0001-9283-0471 (P. Maugis)

field approximation implies the use of average site fractions of carbon  $C_i$  on each sublattice  $i$ , and the consideration of the homogeneous strain  $\epsilon$ , irrespective of the strain heterogeneities. The core of the model is the mathematical expression of the enthalpy of the crystal as function of composition, temperature and applied stress. From the enthalpy function, the migration enthalpy of the carbon atoms is expressed, leading to the rate equations of the site fractions, and by integration, to the time-dependent strain response. The main features of the model are described below.

## 2.1. Equations of the model

Carbon atoms soluted in the bcc lattice sit on the stable octahedral sites. They migrate via the unstable tetrahedral sites. There are 3 non-equivalent octahedral configurations (labelled  $i = 1, 2, 3$ ) and 3 non-equivalent tetrahedral configurations (labelled  $j = 1, 2, 3$ ). Each configuration is characterised by its force dipole tensor  $\mathbf{P}^{O_i}$  or  $\mathbf{P}^{T_j}$  representing the elastic field induced by the defect. In our mean-field approach, each carbon atom interacts with the elastic field created by both the applied stress and the other carbon atoms. The resulting homogeneous strain tensor  $\epsilon$  is expressed as a function of the stress tensor  $\sigma$  and of the force dipole density tensor  $\mathbf{p}$  [26]:

$$\epsilon = \mathbf{S}(\sigma + \mathbf{p}). \quad (1)$$

$\mathbf{S}$  is the elastic compliance tensor of the crystal. The dipole density  $\mathbf{p}$  depends on the distribution of the carbon atoms over the sites. When all carbon atoms lie on octahedral sites,  $\mathbf{p}$  is written as

$$\mathbf{p} = \frac{1}{V_0} \sum C_i \mathbf{P}^{O_i}, \quad (2)$$

where  $V_0$  is the atomic volume of the lattice. The dipole density of the crystal varies during and after each carbon jump. For a given distribution of the carbon atoms over the interstitial sites, the elastic contribution to the total enthalpy is then written, for a crystal of volume  $V$ ,

$$H = -\frac{1}{2} V \mathbf{S}(\sigma + \mathbf{p}) \cdot (\sigma + \mathbf{p}). \quad (3)$$

As an equivalent to the force dipoles tensors, we introduce the strain dipole tensors  $\lambda = \mathbf{S}\mathbf{P}/V_0$ . According to the tetragonal symmetry of the defects, each of these tensors has a singlet component  $\lambda_1$  representing the strain induced by a carbon atom along the tetragonal axis, and a doublet component  $\lambda_2$  representing the strain in perpendicular directions. With these notations, and making use of Equation 3, the migration enthalpy of a carbon atom from site  $i$  through the transition site  $j$  is written [17]

$$H_{i \rightarrow j}^m = H_0^m - V_0 (\lambda^{T_j} - \lambda^{O_i}) \cdot (\sigma + \mathbf{p}), \quad (4)$$

where  $H_0^m$  is the migration enthalpy in the stress-free carbon-free crystal. It is clear from this equation that not only the applied stress but also the carbon distribution affect the migration enthalpy.

According to the jump rate theory, the probability per second for a carbon atom to jump from stable site  $i$  through the transition site  $j$  is written

$$p_{i \rightarrow j} = \nu_0 \exp \left( -H_{i \rightarrow j}^m / k_B T \right). \quad (5)$$

From this probability function, two means of time integration are available. The first one is the Monte Carlo method. On-lattice atomic kinetic Monte Carlo (AKMC) was applied successfully to study the thermodynamic [17], thermo-elastic [26], diffusional [18] and relaxation [21] properties of the Fe-C system. Details of the method can be found in reference [17].

The second means of time integration is the mean-field approach used in the thermo-kinetic model. In this approach, the jump frequency from  $i$  through  $j$  is written  $\Gamma_{i \rightarrow j} = C_i p_{i \rightarrow j}$ . The net flux from stable position  $i$  to stable position  $k$  via the saddle position  $j$  is then  $J_{i \rightarrow k} = \Gamma_{i \rightarrow j} - \Gamma_{k \rightarrow j}$ . An octahedral site of type  $i$  has two nearest neighbours of type  $k$  and two nearest neighbours of type  $k'$ . Then the matter balance at site  $i$  implies the rate equations

$$\dot{C}_i = 2 (J_{k \rightarrow i} + J_{k' \rightarrow i}), \quad i = 1, 2, 3. \quad (6)$$

These equations are conservative, such that the total carbon fraction  $C = \sum C_i$  remains constant. When integrated, the coupled equations (6) provide the time evolution of the site fractions  $C_i(t)$  under given applied stress. The resulting strain response is provided by Equation 1.

In Section 3, the thermo-kinetic model is compared to Monte Carlo simulations.

## 2.2. The linear-response approximation

When the applied stress is low, the strain response is also low, unless certain circumstances discussed later. Then the strain response is accurately approximated by a linear function of the stress. Similarly to reference [21], we used this approximation to model the internal friction in a forced torsion pendulum experiment. We considered a crystal submitted to a pure (001)[110] shear stress such that  $\sigma_{22} = -\sigma_{11} = \sigma(t)$ . The crystal response to a sinusoidal excitation of pulsation  $\omega$  is a sinusoidal pure shear strain  $\epsilon(t) = \epsilon_{22} - \epsilon_{11}$ . The time lag between stress and strain corresponds to the energy loss  $Q^{-1}$ , which follows a Debye curve [29]:

$$Q^{-1} = \Delta \frac{\omega \tau}{1 + (\omega \tau)^2} \quad (7)$$

From our thermo-kinetic model, we established the equations relating the relaxation strength  $\Delta$  and the relaxation time  $\tau$  to the carbon content [21]. The calculated relaxation strength is a non-linear function, exhibiting a singularity at  $C = C^-$ :

$$\Delta(C) = \frac{C}{C^- - C} \quad (8)$$

Carbon fraction  $C^-$  is the value above which the solid solution becomes unstable relatively to Zener ordering. It depends linearly on temperature as

$$C^- = \frac{3S'}{2V_0(\lambda_1 - \lambda_2)^2} k_B T. \quad (9)$$

This equation defines a spinodal line in the temperature–composition phase diagram. We introduced the shear compliance  $S' = 2(S_{11} - S_{12})$ . The compression compliance will also be of use:  $S'' = S_{11} + 2S_{12}$ .

The relaxation time exhibits the same singularity as the relaxation strength:

$$\tau(C) = (6\nu_0)^{-1} \exp \left[ \frac{H_0^m + E_{\text{HZ}}C}{k_B T} \right] \frac{C^-}{C^- - C} \quad (10)$$

where  $\nu_0$  is the attempt frequency for carbon migration and  $H_0^m$  is the migration enthalpy in the infinite dilution limit. The novelty of our approach is the expression of the composition-dependent activation enthalpy of the relaxation time:

$$H^m = H_0^m + E_{\text{HZ}}C, \quad (11)$$

with

$$E_{\text{HZ}} = -\frac{V_0}{3S''} \text{tr}(\lambda^0) \text{tr}(\lambda^T - \lambda^0). \quad (12)$$

The energy coefficient  $E_{\text{HZ}}$  depends only on the elastic properties of the material. It originates from the effect of strain (both volumic and shear components) on the migration enthalpies of the interstitials [18]. Notice that in the limit of low carbon content ( $C \rightarrow 0$ ) one recovers from Equation 10 the usual expression of the Snoek relaxation time  $\tau^{-1} = 6\nu_0 \exp(-H_0^m/k_B T)$ . The consequences of the composition dependence of  $\Delta$  and  $\tau$  are (i) the giant Snoek relaxation in the vicinity of the ordering transition and (ii) the shift and broadening of the Snoek peak in frequency-dependent internal friction [21]. Such effects are investigated further in Section 3.

In order to explore the influence of temperature, we can alternatively express the relaxation strength and time as functions of  $T$ . Actually, by substituting  $C^-$  (Eq. 9) into Eqs. 8 and 10, the relaxation strength is written

$$\Delta(T) = \frac{T^-}{T - T^-} \quad (13)$$

and the relaxation time

$$\tau(T) = (6\nu_0)^{-1} \exp \left[ \frac{H_0^m + E_{\text{HZ}}C}{k_B T} \right] \frac{T}{T - T^-} \quad (14)$$

with temperature  $T^-$  defined by

$$k_B T^- = \frac{2V_0(\lambda_1 - \lambda_2)^2}{3S'} C. \quad (15)$$

In the vicinity of  $T = T^-$  the relaxation strength  $\Delta(T)$  diverges with the power law  $(T - T^-)^{-1}$ . However, this produces no divergence of the energy loss because the relaxation time  $\tau(T)$  diverges with the same law. Hence, in the vicinity of  $T^-$  the increase in relaxation strength is canceled out by the increase in relaxation time. As a result, the linear-response approximation predicts no discontinuity in energy

loss when crossing  $T^-$ :

$$Q^{-1}(T^-) = \frac{6\nu_0}{\omega} \exp \left[ \frac{S'}{2S''} \frac{\text{tr}(\lambda^0) \text{tr}(\lambda^T - \lambda^0)}{(\lambda_1 - \lambda_2)^2} \right] \times \exp \left[ -\frac{H_0^m}{k_B T^-} \right]. \quad (16)$$

Such a property was previously described by Nowick and Berry [29]. It will be further discussed in Section 4.2.

### 2.3. Model parameters and computation set up

We assumed that the material parameters do not depend on temperature in the range of interest (250–400K). We used the lattice parameter, elastic stiffness tensor and force dipole tensors computed from first principles in reference [18], such that they are consistent with one another. The values are reported in Table 1, together with the symmetrised compliances and the strain dipole tensors deduced from the elasticity theory. The values are compatible with the data found in the literature. The attempt frequency and migration enthalpy for carbon were fitted to the data of da Silva [30]:  $\nu_0 = 159$  THz and  $H_0^m = 0.872$  eV.

The phase diagrams were constructed by minimising the Gibbs energy function  $G = H - TS$ .  $H$  is the enthalpy function of Equation 3 and the  $S$  is the configurational regular entropy.

Snoek relaxation profiles were obtained from successive computations of the thermo-kinetic model at selected frequencies  $f = \omega/2\pi$ . High-accuracy Runge-Kutta integration of the rate equations was performed to get the time-dependent site fractions. The internal friction is defined as the fractional energy loss per cycle:

$$Q^{-1} = \frac{1}{2\pi} \frac{\delta W}{W}. \quad (17)$$

$W$  is the maximum elastically stored energy per unit volume during a cycle.  $\delta W$  was computed as the integral of  $\sigma \cdot d\epsilon$  along a cycle. When varying the temperature for internal friction computations, the starting state of the alloy was set to fully disordered. In doing so, we simulated internal friction measurements upon cooling of the ferrite phase.

### 2.4. Comparison with experiment

As a test of the thermo-kinetic model, we compared our results with the temperature-dependent internal friction measurements of Weller [31]. They were performed on a 20 at.ppm C polycrystal at the oscillation frequency of 1 Hz. The internal friction computed on a single crystal was converted to the polycrystal response via the Reuss averaging method [29, 32] according to the relationship

$$Q_{\text{poly}}^{-1} = \frac{2S'}{5G^{-1}} Q_{\text{single}}^{-1} \quad (18)$$

where  $G^{-1} = (3/5)S_{44} + (2/5)S'$  is the average inverse torsion modulus. With the data of Table 1, we have  $Q_{\text{poly}}^{-1} = 0.516 Q_{\text{single}}^{-1}$ . Comparison with experiment is satisfactory, given that no fitting parameter was used (Fig. 1)

**Table 1**

Top rows: lattice parameter  $a_0$  (in nm), elastic compliances  $S_{ij}$  (in  $\text{GPa}^{-1}$ ) and dipole moments  $P_a$  and  $P_c$  (in eV) computed by DFT. Bottom rows: symmetrised compliances (in  $\text{GPa}^{-1}$ ) and dipole strains deduced from elasticity theory.

$a_0$	$S_{11}$	$S_{12}$	$S_{44}$	$P_c^O$	$P_a^O$	$P_c^T$	$P_a^T$
0.2855	0.00615	-0.00218	0.0104	17.0	10.0	5.37	14.8
				$\lambda_1^O$	$\lambda_2^O$	$\lambda_1^T$	$\lambda_2^T$
				0.838	0.0350	-0.435	0.647

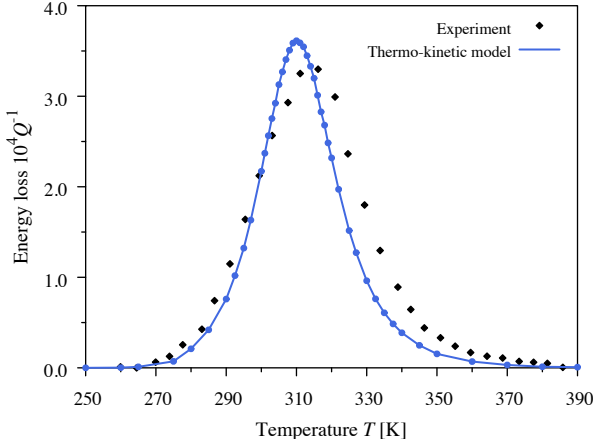


**Figure 1:** Snoek relaxation profile calculated from the thermo-kinetic model (continuous line, circles) compared to the experiment of Weller [31] (diamonds). The alloy is Fe-20 at.ppm C, the oscillation frequency is 1 Hz.

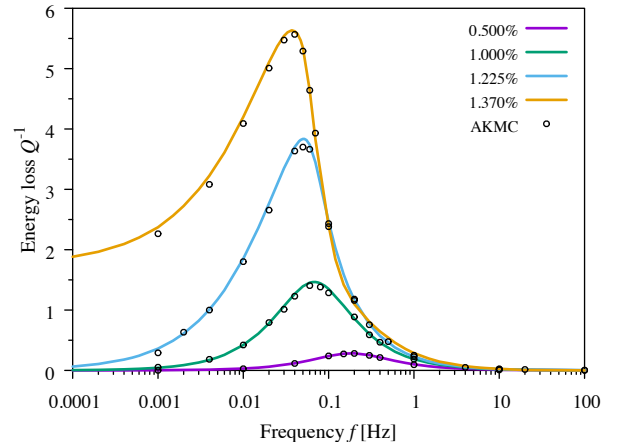
### 3. Frequency-dependent internal friction

Frequency-dependent internal friction is usually measured at room temperature in a series of runs at various oscillation frequencies. Figure 2 presents a set of Snoek profiles computed with the thermo-kinetic model at temperature  $T = 300$  K over a wide range of oscillation frequency. Specific carbon contents have been selected:  $C = 0.5\%$  is just beyond the limit of the composition–peak height linear relationship;  $C_0 = 1.225\%$  coincides with the Zener order-disorder transition; and  $C = 1.37\%$  is close to the spinodal composition of  $C^- = 1.379\%$  (Eq. 9). We see in Figure 2 that the peak height increases rapidly with increasing carbon content, while the peak position shifts towards lower frequencies. The profiles also appear broadened and skewed at high carbon content.

These results are compared to kinetic Monte Carlo simulations reported in reference [21]. The simulations used an applied stress amplitude of 100 MPa, a high value as reference to experimental usage, but technically necessary to overcome the high fluctuations present in the finite-size simulation box. The coincidence between both approaches is very good, which validates the thermo-kinetic model. The later has the advantage of being far less computationally demanding than the Monte Carlo simulations.

The steep increase in peak height when  $C$  approaches

1.379% is a manifestation of the giant Snoek effect in the vicinity of the spinodal point. The correlative skewness of the profile is well rendered by the thermo-kinetic model. Such a behaviour could not emerge from the linear-response approximation since the later, although incorporating the singularity at  $C = C^-$ , keeps a Debye dependency on the frequency.



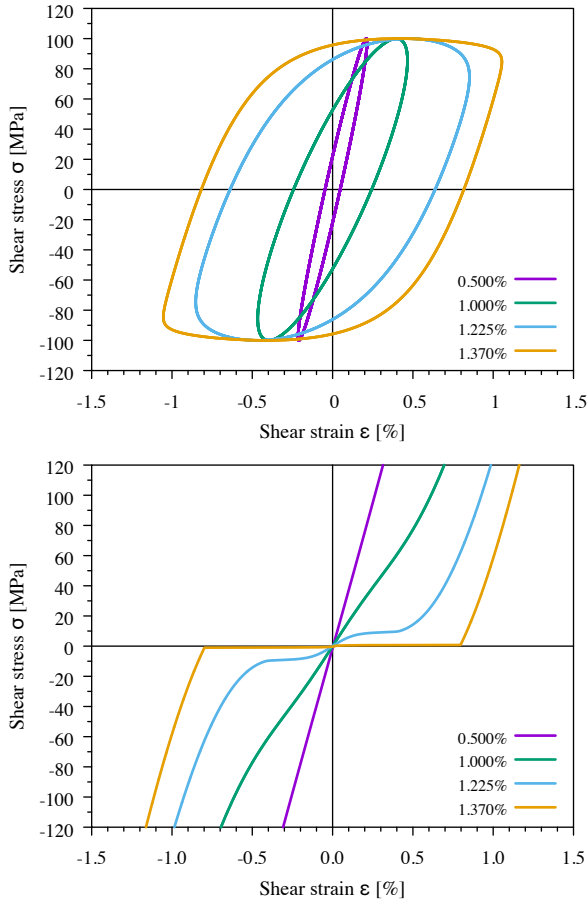
**Figure 2:** Snoek relaxation profiles for various compositions computed with the thermo-kinetic model (lines) compared to the simulations by kinetic Monte Carlo (circles) [21]. The temperature is  $T = 300$  K.

Figure 3, top gathers the stress–strain hysteresis cycles corresponding to the peak frequencies of Figure 2. The cycle at  $C = 0.5\%$  has an ellipsoid shape, as expected in the linear regime. When the carbon content increases, the cycle grows and its largest diagonal declines. This decline corresponds to an effective softening of the alloy. Correlatively, the cycle area increases largely, in direct relation with the increase in energy loss.

The very large energy loss when  $C$  approaches  $C^-$  can be understood from the quasi-static stress–strain isotherms drawn in Figure 3, bottom. These curves have been computed with a very small stress rate insuring equilibrium at each time step, starting from the disordered state at  $\sigma = 0$ . Close to the linear regime ( $C = 0.5\%$ ), the stress–strain characteristic is almost a straight line, whose slope is slightly less than the inverse shear compliance  $1/S'$ . When the carbon content increases, the characteristic becomes non linear and the slope at low stress continues to decrease. At  $C = 1.37\%$ ,



the curve is almost flat in the strain range of  $[-0.79\%, 0.79\%]$  under low applied stress, and steep beyond. Such a superelastic behaviour is due to the collective migration of the carbon atoms towards the favoured interstitial sites. The carbon atoms induce a large anelastic strain at little stress expense (0.74 MPa). This arises because the disorder to order transition becomes barrier-less when the spinodal line is reached. Consequently, the static compliance is almost infinite. Under dynamic conditions, the corresponding energy loss is naturally very large, as seen in Figure 2.



**Figure 3:** Top: stress-strain hysteresis cycles corresponding to the peak frequencies of Figure 2. Bottom: quasi-static stress-strain isotherms.

## 4. Temperature-dependent internal friction

Temperature-dependent internal friction is obtained experimentally by a series energy-loss measurements performed at various temperatures. The resulting profiles depend on the oscillation frequency. We will show that they are strongly carbon-dependent. The results will be discussed in relation to the thermo-elastic properties of the Fe-C system.

### 4.1. The thermo-elastic properties of Fe-C

During a temperature-dependant internal friction measurement, the thermo-elastic properties of the material are

scanned over a range of temperature. Zener ordering may occur in that range, to which the Snoek relaxation is sensitive. In the present work, we focused on carbon-supersaturated alloys, i.e. carbon is assumed to remain in solid solution. This can be achieved in practice by measuring the Snoek profile during cooling from a not too elevated temperature. Under this condition, the thermo-elastic properties of the alloy are expected to evolve strongly in the vicinity of the ferrite to martensite transition temperature [33].

To investigate this point and shed light on the giant relaxation phenomenon in temperature-dependant internal friction measurements, the temperature-stress phase diagram and the stress-strain isotherms we computed in the case of a carbon content  $C = 1.37$  at.% (0.30 wt.%).

The stress-composition phase diagram drawn in Figure 4 was constructed by minimisation of the Gibbs energy. The first-order transition lines form a symmetric Y-shape. At high temperature, the ferrite phase is stable. It is characterised by a low degree of Zener order (total disorder is achieved at zero stress). The martensite phase is stable at low temperature. It has a high degree of Zener order, i.e. most carbon atoms sit on one type of octahedral sites. Zener order-disorder transitions occur along the inclined transition lines, which join at zero-stress and temperature  $T_0 = 322$  K.  $K$  and  $K'$  are two critical points beyond which the order-disorder transition is continuous ( $\sigma_{K'} = -\sigma_K = 9.04$  MPa and  $T_K = T_{K'} = 335$  K). An important point for the thermo-elastic behaviour of the alloy is the spinodal point at zero stress, located at temperature  $T^- = 298$  K.

When the temperature is decreased, under zero-stress condition, the ordering transition can occur below  $T_0$ . However, disorder may persist as a metastable state until temperature  $T^-$  (Eq. 15) is reached, at which stage the ordering transition occurs barrier-less. The stress-composition phase diagram is homothetic in carbon content, i.e. a diagram at composition  $C$  can be deduced from Figure 4 by rescaling both axes proportionally to  $C$ .

The thermo-elastic behaviour is related to the temperature-stress phase diagram. Selected stress-strain isotherms of the alloy  $C = 1.37$  at.% are gathered in Figure 4, bottom. Notice that the stress axis is horizontal, and coincides with the phase diagram on top. At  $T = 400$  K, a temperature far above the ordering transition, the stress-strain characteristic is almost linear, with a slope slightly higher than the shear compliance  $S'$ . When the temperature is decreased, strong non-linearities appear, together with an increase in slope at the origin. At the temperature of the critical points,  $T_K$ , the slope is infinite when the stress equals the critical value of  $\pm 9.04$  MPa corresponding to the critical points  $K$  and  $K'$ . Below  $T_K$ , a step in strain accompanies the order-disorder transition when crossing the  $K'T_0K$  line. The amplitude of the step is maximum at the spinodal temperature ( $T^-$ ). At this temperature, a vanishing stress produces a finite strain, i.e. the static compliance is infinite, as expected at a critical point [1, 34].

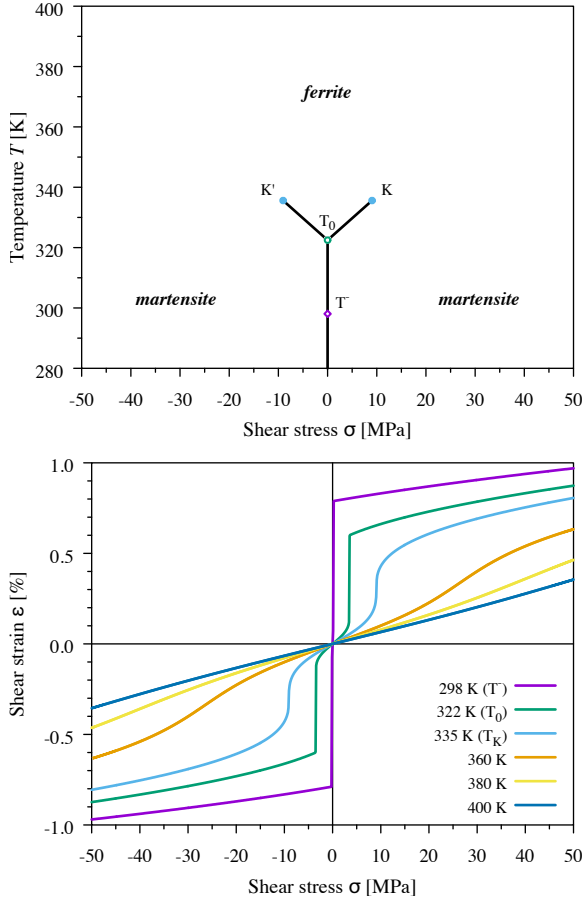


**Figure 4:** Top: temperature–stress phase diagram computed at carbon content  $C = 1.37\%$ . The spinodal point lies at  $\sigma = 0$  and  $T^- = 298$  K. Bottom: stress-strain isotherms computed at  $C = 1.37\%$ . Note that the stress axis is horizontal in both graphs.

#### 4.2. Influence of the oscillation frequency

The computer implementation of the thermo-kinetic model allows for fast computation of low-frequency and low-stress simulations. The stress amplitude was set to 1 MPa in a series of computations where the oscillation frequency  $f$  was varied from  $10^{-2}$  to 100 Hz. We obtained the profiles presented in Figure 5.

As expected for thermo-activated processes, the peak position shifts toward low temperatures when decreasing the frequency, while the peak height increases. The high-frequency profiles ( $f \geq 1$  Hz) are well reproduced by the linear-response approximation. In this regime, the system is driven out-of-equilibrium at a frequency that does not allow enough time for the ordering transition to take place, although the temperature is brought below  $T_0$ . This is not the case at lower frequencies ( $f \leq 10^{-1}$  Hz). In particular, at  $f = 10^{-2}$  Hz the sharp drop in energy loss located at 307 K is caused by the ferrite to martensite transition. Such a transition is a non-linear effect, out of reach of the linear model [29].

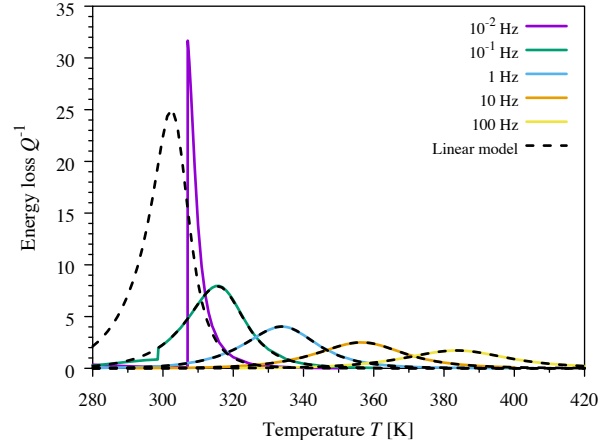


**Figure 5:** Snoek relaxation profiles computed with the kinetic model at various oscillation frequencies (lines) compared to the linear model (dashed lines), for  $C = 1.37\%$ . The linear model fails in the low-frequency regime.

#### 4.3. Effect of carbon content

The effect of carbon content was studied at the usual oscillation frequency of 1 Hz. The linear model proved to be a good approximation at this frequency. It was run for carbon contents up to 1.37 at.% (Fig. 6).

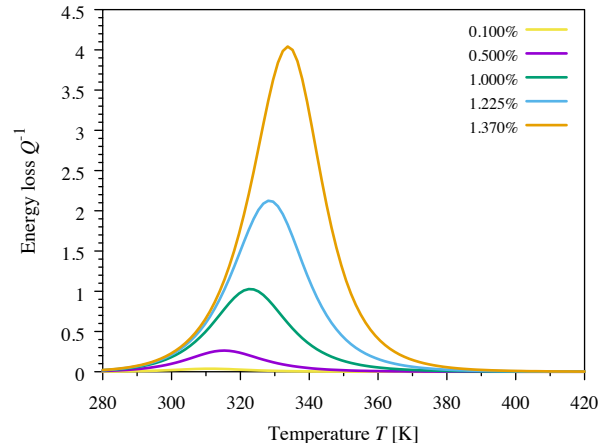


**Figure 6:** Snoek relaxation profiles for various carbon contents computed with the linear model. The oscillation frequency is  $f = 1$  Hz.

Two important features emerge. First, the peak height is a steep function of carbon content in the vicinity of 1.4 at.%, as can be seen in Figure 7. The peak-height–carbon content relationship is linear only for carbon content as low as  $\sim 0.2$  at.%, similarly to the frequency-dependent case (see Section 3).

Second, the peak position is composition-dependent: it is equal to 310 K at low carbon but shifts towards higher temperatures when the carbon content increases, up to 334 K when  $C = 1.37\%$  (Fig. 7). Given the temperature dependence of both  $\Delta(T)$  and  $\tau(T)$  (Eqs. 13, 14 and Fig. 8), the peak coordinates are not analytical. The shift can nevertheless

less be qualitatively understood from the increase in activation enthalpy  $H^m$  with carbon content (Eq. 11): numerically  $H^m = 0.872 + 0.600C$ , which varies from 0.872 to 0.880 eV in the range of  $C = 0$  to  $C = 1.37\%$ .

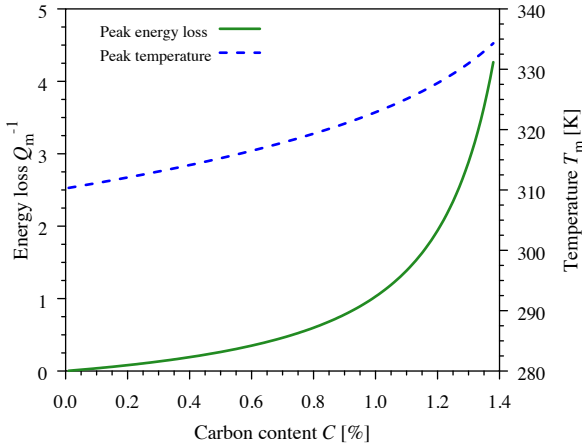


**Figure 7:** Peak energy loss and peak temperature of the Snoek profile as functions of carbon content, computed from the linear model.  $f = 1$  Hz.

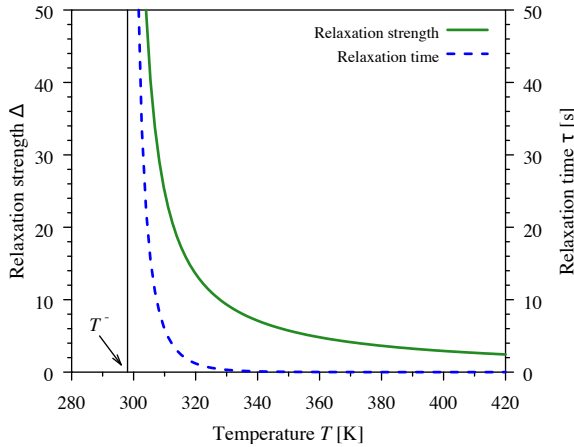


**Figure 8:** Relaxation strength and relaxation time computed from the linear model at carbon content  $C = 1.37\%$ . Both functions diverge at temperature  $T^- = 298$  K (vertical line).

## 5. Discussion

The thermo-kinetic model predicts that the peak energy loss in internal friction measurements should reach huge values when the carbon content is close to the Zener order-disorder transition. This giant Snoek relaxation is non-linear with respect to the carbon content. It is accompanied by a shift in the peak position in frequency-dependent and temperature-dependent experiments.

Such a behaviour was previously identified by Monte-Carlo simulations of frequency-dependent internal friction [21]. For technical reasons, the Monte-Carlo simulations were restricted to high stress amplitudes (100 MPa). Such

amplitudes are more in line with the hysteretic damping phenomenon than with internal friction. Conversely, the thermo-kinetic model allows for small stress amplitudes. The present work shows that the above-mentioned relaxation properties are kept with stress amplitudes as low as 1 MPa. Our model has also the advantage of being very fast running, which allows for an easier study of the low-frequency regime.

Our understanding of the non-linear effects on Snoek relaxation is in line with Zener's theory [20]. It is at variance, however, to some previous approaches. Based on a Ginzburg-Landau approximation, Nowick and Berry studied theoretically the energy-loss singularity in the vicinity of a *second-order* transition, which is of Curie-Weiss type [29, 35]. Our approach is closer to that of Dattagupta et al. [22], who recognised that the Zener order-disorder transition is a *first-order* transition. Our mathematical treatment is somewhat simpler than Dattagupta's. It clarifies one point: giant relaxation is related to the *spinodal* temperature  $T^-$  via the diverging term  $(T - T^-)^{-1}$ , whereas the sharp peak at low frequency is related to the *transition* temperature  $T_0$ . In the Fe-C system, these temperatures can be separated by 15 K or more, depending on the carbon content.

Comparison between the thermo-kinetic model and the linear-response theory highlights the limits of the linear approximation. Actually, only a non-linear approach can capture the influence of the order-disorder transition on the low-frequency response. In simple words, the linear model does not know the order-disorder transition, although it knows the spinodal point.

The non-Debye character of our computed Snoek peaks is a manifestation of the so-called "interaction" between the solute atoms [36]. Contrary to the works of Weller et al. [37], Haneczok et al. [25, 38] and Blanter et al. [39–41], the *short-range* interactions are not at work in our approach. The *long-range* elastic interaction between the defect dipoles and the homogeneous strain is rather the origin of both the peak increase and the peak shift. The homogeneous strain is generated by both the applied stress and the carbon-induced strain. As a consequence of the carbon-induced strain, the carbon atoms are not independent: once a carbon atom has moved to a favoured site, it produces a strain that further favours energetically the sites of same type. The resulting autocatalytic effect is all the more pronounced the closer to the order-disorder spinodal. Near the spinodal point, applying a small stress at the adequate frequency is enough to promote a large proportion of carbon atoms into the favoured sites. This collective behaviour of interstitial atoms creates the giant anelastic response. Theories that approximate the total relaxation strength to the sum of individual atomic contributions do not account for this collective behaviour. They can therefore not predict giant relaxation.

The carbon-strain interaction acts not only on the carbon atoms sitting in stable octahedral positions. The interaction also modifies the energetic path of migrating carbon atoms, especially at the tetrahedral unstable position. As a consequence, the activation energy of the relaxation time is composition-dependent. This further raises the relaxation



time at high carbon content, in addition to the effect of the spinodal.

We found that both characteristic temperatures  $T_0$  and  $T^-$  are linear functions of the carbon content. Such a composition dependence was identified experimentally by Haneczok et al. [42] on the so-called critical temperature in the Fe-C system. Besides, a non-linear increase in the peak height was evidenced when increasing solute oxygen in Ta [43]. The origin of this is probably not the same as in our case because the measured curvature of the  $Q_m^{-1}$ -oxygen content curve is opposite to ours. In addition, the dipole tensor of the Ta-O system is probably too weak to produce a measurable effect of the dipole-strain interaction in this system. The experimental confirmation of the non-linear dependence of  $Q_m^{-1}$  on solute carbon in Fe-C is still awaited.

The sharp peak predicted at the crossing of temperature  $T_0$  during cooling is not reported in the literature. Two reasons can explain this: first, according to our calculations the peak only occurs at low-frequency oscillations ( $f \leq 10^{-1}$  Hz), which are rarely used in temperature-dependent internal friction. Second, the calculated peak has a very narrow temperature range, and may be damped out if the cooling rate is too fast. For these reasons, the peak will be difficult to evidence, unless specific means are implemented.

## 6. Conclusion

Based on the elasticity theory of point defects and on the rate theory of thermally activated processes, we built a mathematical model of the kinetics of Snoek relaxation. Its application to frequency-dependent and temperature-dependent internal friction in the Fe-C system showed that the peak in energy loss grows non-linearly with carbon content. In the vicinity of the spinodal of the Zener disorder to order transition, the energy loss exhibits giant values. The peak position is shifted by the thermodynamic effect of the transition and by the kinetic effect of the composition-sensitive carbon migration path.

## Declaration of Competing Interest

The authors declare that they have no known competing financial interests or personal relationships that could have appeared to influence the work reported in this paper.

## Aknowledgements

This work was supported by the Agence Nationale de la Recherche (contract C-TRAM ANR- 18-CE92-0021).

## References

- [1] C. Zener, Theory of strain interaction of solute atoms, *Phys. Rev.* 74 (1948) 639–647.
- [2] M. Shtremel, F. Satdarova, Influence of stresses on order in interstitial solutions, *Fiz. Met. Met.* 34 (1972) 699–708.
- [3] A. Khachaturyan, G. Shatalov, On the theory of the ordering of carbon atoms in a martensite crystal, *Fiz. Met. Met.* 32 (1971) 5–13.
- [4] K. Taylor, M. Cohen, Ageing of ferrous martensites, *Prog. Mater. Sci.* 36 (1992) 225–272.
- [5] P. Chirkov, A. Mirzoev, D. Mirzaev, Tetragonality and the distribution of carbon atoms in the Fe-C martensite: Molecular-dynamics simulation, *Phys. Met. Metallogr.* 117 (2016) 34–41.
- [6] P. Maugis, F. Danoix, H. Zapolsky, S. Cazottes, M. Gouné, Temperature hysteresis of the order-disorder transition in carbon-supersaturated  $\alpha$ -Fe, *Phys. Rev. B* 96 (2017) 214104.
- [7] G. Kurdjumov, A. Khachaturyan, Nature of axial ratio anomalies of the martensite lattice and mechanism of diffusionless gamma to alpha transformation, *Acta Metall.* 23 (1975) 1077–1088.
- [8] Z. Fan, L. Xiao, Z. Jinxiu, K. Mokuang, G. Zhenqi, Lattice-parameter variation with carbon content of martensite. II. Long-wavelength theory of the cubic-to-tetragonal transition, *Phys. Rev. B* 52 (1995) 9979–9987.
- [9] A. Udyansky, J. Von Pezold, V. N. Bugaev, M. Friák, J. Neugebauer, Interplay between long-range elastic and short-range chemical interactions in Fe-C martensite formation, *Phys. Rev. B - Condens. Matter Mater. Phys.* 79 (2009) 224112.
- [10] A. Udyansky, J. von Pezold, A. Dick, J. Neugebauer, Orientational ordering of interstitial atoms and martensite formation in dilute Fe-based solid solutions, *Phys. Rev. B* 83 (2011) 184112.
- [11] X. Zhang, H. Wang, T. Hickel, J. Rogal, Y. Li, J. Neugebauer, Mechanism of collective interstitial ordering in Fe-C alloys, *Nat. Mater.* (2020).
- [12] R. Naraghi, M. Selleby, Stability of Fe-C Martensite-Effect of Zener-Ordering, in: P. C. John Allison, G. Spanos (Eds.), 1st World Congr. Integr. Comput. Mater. Eng., TMS, 2011, pp. 235–240.
- [13] R. Naraghi, M. Selleby, J. Ågren, Thermodynamics of stable and metastable structures in Fe-C system, *Calphad Comput. Coupling Phase Diagrams Thermochem.* 46 (2014) 148–158.
- [14] C. W. Sinclair, M. Perez, R. G. A. Veiga, A. Weck, Molecular dynamics study of the ordering of carbon in highly supersaturated  $\alpha$ -Fe, *Phys. Rev. B* 81 (2010) 224204.
- [15] P. Chirkov, A. Mirzoev, D. Mirzaev, Molecular-dynamics Simulations of Carbon Ordering in bcc Fe and its Impact on Martensite Transition, *Mater. Today Proc.* 2S (2015) 553–556.
- [16] O. Waseda, J. Morthomas, F. Ribeiro, P. Chantrenne, C. W. Sinclair, M. Perez, Ordering of carbon in highly supersaturated  $\alpha$ -Fe, *Model. Simul. Mater. Sci. Eng.* 27 (2019) 015005.
- [17] P. Maugis, Ferrite, martensite and supercritical iron: A coherent elastochemical theory of stress-induced carbon ordering in steel, *Acta Mater.* 158 (2018) 454–465.
- [18] P. Maugis, S. Chentouf, D. Connétable, Stress-controlled carbon diffusion channeling in bcc-iron: A mean-field theory, *J. Alloys Compd.* 769 (2018) 1121–1131.
- [19] P. Maugis, D. Connétable, P. Eyméoud, Stability of Zener order in martensite: an atomistic evidence, *Scr. Mater.* 194 (2021) 113632.
- [20] C. M. Zener, Elasticity and anelasticity of metals, The University of Chicago Press, 1948.
- [21] P. Maugis, Giant Snoek peak in ferrite due to carbon-carbon strain interactions, *Materialia* 12 (2020) 100805.
- [22] S. Dattagupta, R. Balakrishnan, R. Ranganathan, Strain ordering in BCC metals and the associated anelasticity, *J. Phys. F* 12 (1982) 1345–1362.
- [23] S. K. Ghoshal, S. Dattagupta, 3-d Model for strain ordering in steel: II relaxational effects, *Pramana - J. Phys.* 51 (1998) 539–546.
- [24] K. L. Ngai, Y. N. Wang, L. B. Magalas, Theoretical basis and general applicability of the coupling model to relaxations in coupled systems, *J. Alloys Compd.* 211–212 (1994) 327–332.
- [25] G. Haneczok, M. Weller, J. Diehl, Internal Friction Studies on Oxygen-Oxygen Interaction in Niobium, *Phys. status solidi B* 172 (1992) 557–572.
- [26] P. Maugis, Nonlinear elastic behavior of iron-carbon alloys at the nanoscale, *Comput. Mater. Sci.* 159 (2019) 460–469.
- [27] B. Lawrence, C. W. Sinclair, M. Perez, Carbon diffusion in supersaturated ferrite: A comparison of mean-field and atomistic predictions, *Model. Simul. Mater. Sci. Eng.* 22 (2014) 1–17.

- [28] P. Maugis, D. Kandaskalov, Revisiting the pressure effect on Carbon migration in iron, *Mater. Lett.* 270 (2020) 127725.
- [29] A. S. Nowick, B. Berry, Anelastic relaxation in crystalline solids, *Materials science series* [v. 1], Academic Press, New York, 1972.
- [30] J. da Silva, R. B. McLellan, Diffusion of carbon and nitrogen in B.C.C. iron, *Mater. Sci. Eng.* 26 (1976) 83–87.
- [31] M. Weller, The Snoek relaxation in bcc metals-From steel wire to meteorites, *Mater. Sci. Eng. A* 442 (2006) 21–30.
- [32] H. Ino, S. Takagi, T. Sugeno, On the relaxation strength of the Snoek peak, *Acta Metall.* 15 (1967) 29–34.
- [33] P. Maugis, A Temperature–Stress Phase Diagram of Carbon-Supersaturated bcc-Iron, Exhibiting “Beyond-Zener” Ordering, *J. Phase Equilibria Diffus.* 41 (2020) 269–275.
- [34] L. D. Landau, E. Lifshitz, *Statistical physics*, 2nd ed., Pergamon Press, 1969.
- [35] A. S. Nowick, W. R. Heller, Anelasticity and stress-induced ordering of point defects in crystals, *Adv. Phys.* 12 (1963) 251–298.
- [36] M. Blanter, I. Golovin, H. Neuhauser, H.-R. Sinning, *Internal Friction in Metallic Materials*, 1st ed., Springer-Verlag, Berlin Heidelberg, 2007.
- [37] M. Weller, G. Haneczok, J. Diehl, Internal Friction Studies on Oxygen–Oxygen Interaction in Niobium. I. Experimental Results and Application of Previous Interpretations, *Phys. Status Solidi* 172 (1992) 145–159.
- [38] G. Haneczok, Interaction of interstitial solute atoms in bcc metals, *Phil. Mag. A* 78 (1998) 845–855.
- [39] M. S. Blanter, M. Y. Fradkov, Solute interaction and internal friction spectra in solid solutions, *Acta Metall. Mater.* 40 (1992) 2201–2208.
- [40] M. S. Blanter, L. B. Magalas, Strain-induced interaction of dissolved atoms and mechanical relaxation in solid solutions. A review, *Solid State Phenom.* 89 (2003) 115–140.
- [41] M. S. Blanter, V. V. Dmitriev, A. V. Ruban, Interstitial-interstitial interactions in bcc VB group metals: Ab initio calculations, *J. Phys. Chem. Solids* 74 (2013) 716–722.
- [42] G. Haneczok, M. Weller, J. Diehl, Internal Friction Studies of Carbon–Carbon Interaction in Iron, *Mater. Sci. Forum* 121 (1993) 101–107.
- [43] M. Weller, J. Zhang, G. Li, T. Kê, J. Diehl, Internal friction study on the existence of oxygen pairs in interstitial solid solution of tantalum with oxygen, *Acta Metall.* 29 (1981) 1055–1060.